European Congress on Computational Methods in Applied Sciences and Engineering
ECCOMAS 2000
Barcelona, 11-14 September 2000

LESFOIL: A EUROPEAN PROJECT ON LARGE EDDY SIMULATIONS AROUND A HIGH-LIFT AIRFOIL AT HIGH REYNOLDS NUMBER

L. Davidson

Dept. of Thermo and Fluid Dynamics, Chalmers University of Technology
SE-412 96 Göteborg, Sweden, Email: lada@tfd.chalmers.se
web page: www.tfd.chalmers.se/~lada

Key words: LES, wall functions, airfoil, channel flow, LES-RANS, DES.

Abstract. *This paper presents work carried out in the LESFOIL project, which studies Large Eddy Simulations (LES) of the flow around high-lift airfoils, during its first 24 months. The Reynolds number for the selected Aerospatiale A-airfoil is high ($Re = 2.1 \cdot 10^6$ based on the freestream velocity and the chord length). If some kind of near-wall treatment could be used, the near-wall streaks would not be resolved and a much coarser grid could be used in the streamwise and spanwise directions. Two different near-wall treatment methodologies are used in the LESFOIL project, either hybrid LES-RANS (or DES) or wall functions. The angle of incidence is $\alpha = 13.3^o$, and a small separation bubble is, according to experiments, present on the suction side in the trailing edge region. Thus the method for treating the near-wall wall region must be able to handle both attached boundary layer flow, including streamwise pressure gradients, and separated flow.*

Subgrid-scale (SGS) models and parallelized numerical methods are two other subjects covered in the LESFOIL project. SGS models are developed and evaluated in simple flows such as channel flow. The hill flow (Reynolds number $10,000$ based on the hill height) is also used as a test case in which the performance of the wall treatment and SGS models can be evaluated in recirculating flow.

The first part of the paper presents LES of channel flow. The second part presents hill flow computations. In the following section, LES around the A-airfoil is shown and conclusion are drawn in the final section.

1 INTRODUCTION

Computational Fluid Dynamics (CFD) is an important tool in the design of aircraft. For conventional aircraft under cruise conditions, the current generation of CFD codes allows a computer-based design to be achieved with some confidence. The design process of future aircraft requires extensive research and development in CFD. Efficient and accurate CFD methods allow the aircraft industry to reduce extensive experimental testing, which usually is very expensive. CFD will also allow faster development of new aircraft and modification of existing aircraft, as it may be sufficient to use measurements only in the later stages of development.

To perform accurate numerical simulations of such complex flows, new and more advanced turbulence models are needed. In the LESFOIL project, the feasibility of the application of Large Eddy Simulations (LES) to aerodynamic flows will be assessed, both with aspect to the reliability of the results and the computer resources needed for the calculations.

The main objectives of the project are:

- to provide know-how of an advanced CFD method to the European aeronautical industry;
- to determine when LES will be feasible for the European aeronautical industry;
- to demonstate the feasibility of LES of flow over an airfoil;
- to assess the computational requirements to carrying out LES for the simple airfoil and for more complex configurations in future;
- to develop highly efficient numerical methods for the LES of airfoil flows;
- to compare competing subgrid-scale models for these flows.

The work is divided into five main tasks.

Task 1: Development of subgrid models. If reliable subgrid models are developed, it would be possible to model a larger portion of the turbulence, allowing coarser grids.

Task 2: Near-wall treatment. At high Reynolds numbers, LES requires a fine grid in all three coordinate directions. Use of wall functions or simple RANS (Reynolds Averaging Navier-Stokes) turbulence models in the near-wall region will be studied. This would allow us to use coarser grid spacing, especially in the streamwise and spanwise directions.

Task 3: Transition. In airfoil flow, transition occurs on both the suction and pressure sides. For a correct development of the boundary layer on the suction side, it is crucial to trip transition in a correct way.

Task 4: Development of efficient numerical parallel methods. LES is computationally very expensive, and it is thus extremely important to reduce the computation time as much as possible.

Task 5: LES of airfoil flow. In this task the experience gained in Tasks 1–4 is put together.

Nine parters work in the LESFOIL project, which is coordinated by Chalmers. The partners are (with the researcher in charge in parentheses):

1. Chalmers, Sweden (L. Davidson)
2. Alenia, Italy (N. Ceresola)
3. CERFACS, France (F. Ducros)
4. Dassault, France (M. Mallet)
5. Fluent Europe Ltd, UK (D. Cokljat)
6. Karlsruhe University, Germany (W. Rodi)
7. ONERA, France (T.H. Le)
8. University of Surrey, UK (P. Voke)
9. UMIST/QMW, UK (M.A. Leschziner)

The LESFOIL project started on the 1st of February 1997. This paper presents the outcome of some of the cooperative work carried out thus far in the LESFOIL project. Most of the figures and discussions below have been taken from progress reports written by the partners in the LESFOIL project.

2 CHANNEL FLOW

Some work in the LESFOIL project has been carried out studying channel flow. Simulations of this flow are fairly cheap and can be carried out on workstations or PCs. Because the required CPU time is reasonable, parametric studies have been done in the project investigating different grids, subgrid models and wall models. The experience gained from this simple flow is expected to be valuable in airfoil simulations. Although the channel flow is geometrically very simple, it is a wall-bounded flow in which the near-wall turbulence must be properly predicted in order to perform accurate simulations. In airfoil flow, the attached flow along the suction side prior to separation shares many features of channel flow, although the boundary layer in the former case experiences both favourable and adverse pressure gradients, which are absent in channel flow.

2.1 Wall-resolved Computations

Coarse grid simulations can be considered meaningless since large turbulent structures in the near wall layer cannot be captured. Nevertheless the resolution is representative of the resolution used in some regions of the airfoil flow calculation. It is thus worth checking how subgrid scale models behave on such a poor grid, which, in addition, contains high aspect ratio cells.

CERFACS [1] has used several grids in simulations with the localized dynamic model [2]. Profiles of mean velocity and rms fluctuations shown in Fig. 1 show the improvement in the results when the grid is refined. This is rather reassuring but also proves that the subgrid scale model does not completely fulfil its duty: one could expect results to be insensitive to the grid resolution, the subgrid scale model taking on a greater portion of the job as the grid is coarsened. This is not the case for the range of resolution considered. Actually, the opposite occurs, as shown in Fig. 2. The subgrid scale dissipation provided by the model is actually higher in the finer grid simulation. Eddy-viscosity profiles are interesting: in the region where grids are certainly too coarse to resolve the large eddies, ν_t is stronger on the finer grid but, for $y^+ > 50$, as the grids become more adequate, the expected behaviour is recovered, ν_t being stronger on the coarser grid.

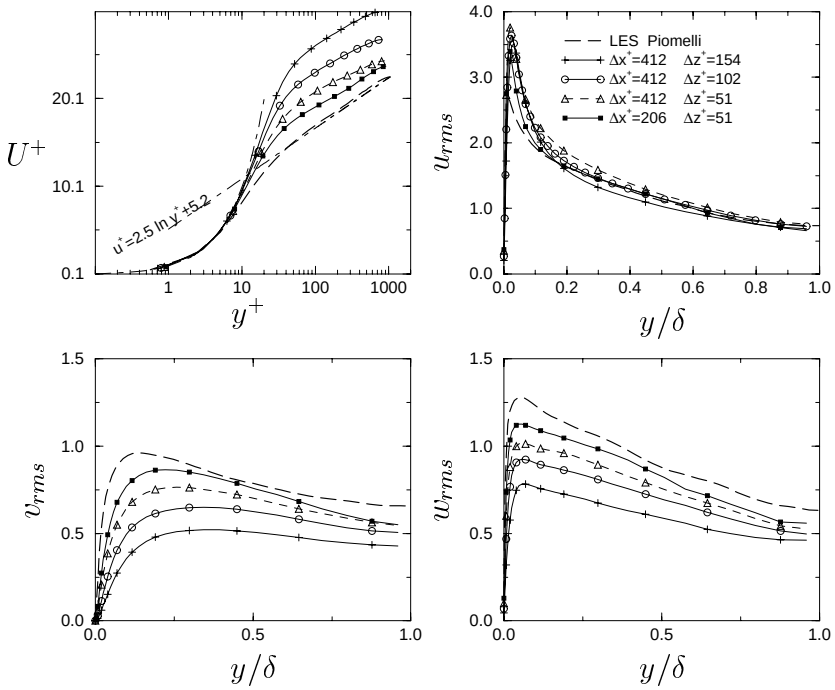

Figure 1: $Re_\tau = 1050$. Profiles of streamwise velocity and of root-mean-square velocity fluctuations in simulations with the localized dynamic model. Grid spacings in the wall normal direction are $\Delta y^+ = 2 - 86$. Results from Ref. [1].

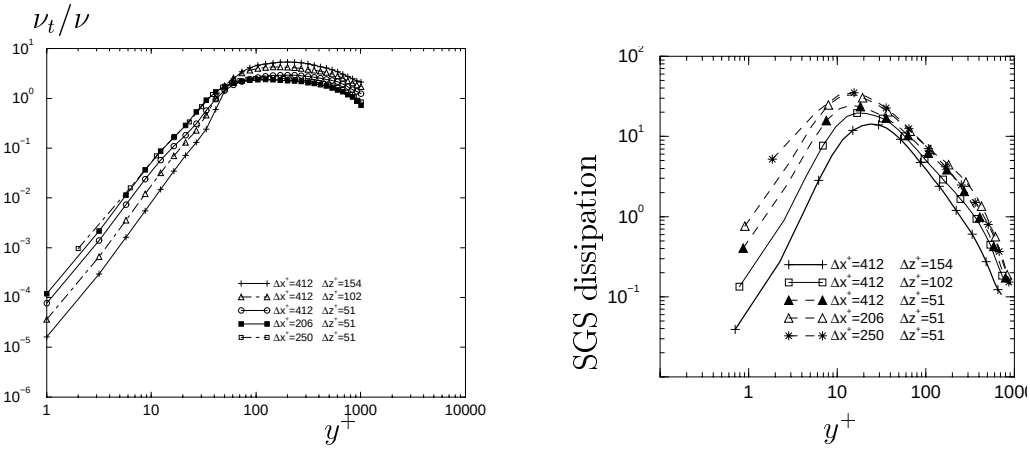

Figure 2: $Re_\tau = 1050$. Localized dynamic model. Left: Profiles of time-averaged eddy-viscosity. Right: Profiles of time-averaged modeled subgrid scale dissipation. Results from Ref. [1].

Figure 3 shows Chalmers' predictions. The dynamic one-equation model by Davidson [3] (see also Ref. [4]) was employed, in which an equation is solved for the subgrid kinetic energy (see Eq. 2). The coefficients in the production (C) and dissipation (C_*) terms are computed dynamically. To ensure numerical stability, a *constant* value of C in space (C_{hom}) is used in the momentum equations. The idea is to include all local dynamic information through the source terms of the transport equation for k_{sgs}. In this way, large fluctuations in the dynamic coefficients are smoothed out in a natural way and the need to restrict or limit the dynamic coefficients is eliminated altogether.

The sensitivity to the grid presented in Fig. 3 exhibits the same trend as the predictions made with the Dynamic SGS model in Fig. 1.

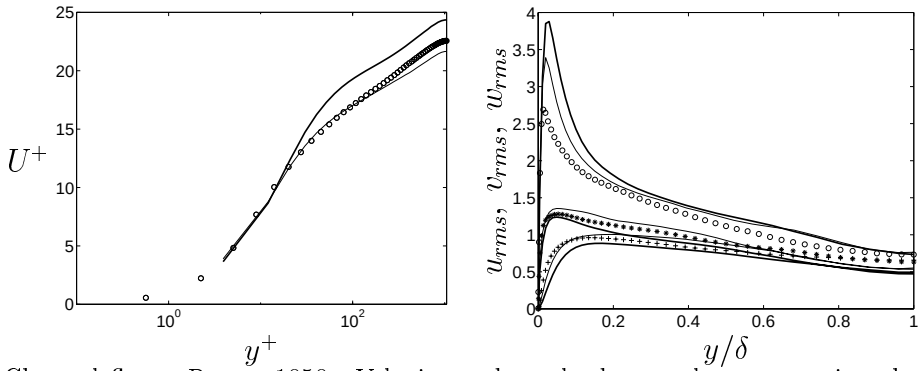

Figure 3: Channel flow. $Re_\tau = 1050$. Velocity and resolved normal stresses using the dynamic one-equation model [3]. $\Delta x^+ = 200$, $\Delta y^+ = 3.9 - 85$. Thick lines: $\Delta z^+ = 50$; thin lines: $\Delta z^+ = 25$. Results from Ref. [5].

2.2 Wall functions

The Reynolds number for the selected Aerospatiale A-airfoil is high ($Re = 2.1 \cdot 10^6$ based on the free stream velocity and the chord length). A wall-resolved mesh based on $\Delta x^+ \simeq 100$ (streamwise direction), $\Delta y^+_{min} \simeq 1$ (wall-normal direction) and $\Delta z^+ \simeq 20$ would require a mesh of approximately $2000 \times 100 \times 300 = 60$ million cells, which is unrealistic. If instead some kind of near wall treatment can be used, in which the near-wall streaks would not be resolved but modelled altogether, a much coarser grid could be used in the streamwise and spanwise directions. By increasing the grid size, time step constraints are also considerably alleviated. Two different near-wall treatment methodologies are used in the LESFOIL project, either a hybrid LES-RANS (or DES) or wall functions. For both methodologies, the required cell spacing would be $100 < \Delta x^+ < 600$ and $100 < \Delta z^+ < 300$. The cell spacing in the wall-normal direction would be much the same as for RANS computations, i.e. $\Delta y^+ \simeq 1$ or $\Delta y^+ \simeq 30$ (near-wall node) for a near-wall RANS method and wall functions, respectively.

In the airfoil flow chosen in the LESFOIL project, a small separation bubble is, according to experiments, present on the suction side in the trailing edge region. Thus the method for treating the near-wall wall region must be able to handle both attached boundary layer flow including streamwise pressure gradients as well as separated flow. While developing such a method is a formidable task that cannot be expected to be accomplished in the LESFOIL project, a first attempt will be made.

In the LESFOIL project, two different wall functions, the law of the wall and the Werner-Wengle wall function, are used. Both wall functions are formulated in instantaneous quantities. The Werner-Wengle wall function uses a power fit of the logarithmic law and allows an explicit evaluation of the friction velocity. Use of a wall function allows placement of the first point well above the wall ($y^+ \simeq 30$).

Karlsruhe [6] evaluated the performance of the dynamic SGS model on stretched and distorted grids. The Werner-Wengle wall function [7] provides the near-wall treatment and the dynamic model the SGS stresses. DNS of Moser *et al.* [8] is used as reference data. A $222 \times 38 \times 66$ node grid is used and is $8\pi \times 2 \times \pi$ units in size. Periodic boundary conditions are applied in the streamwise and spanwise directions. Wall normal and spanwise cell sizes are constant at $\Delta y^+ = 30$ and $\Delta z^+ = 60$, respectively. In the streamwise direction, the grid is divided into five different regions. Regions AB and EF contain cells of streamwise size $\Delta x^+ = 30$. The cells in region CD are also of uniform size with $\Delta x^+ = 220$. The cells in regions BC and DE are either stretched or compressed in the streamwise direction at a rate of 5%. Regions AB and EF are π long, while regions BC, CD and DE are each approximately 2π in length.

Figure 4 shows some results from the computation undertaken with the 5% stretched/compressed grid. It can be seen that the grid stretching/compressing has an impact on the time-averaged statistical data. The mean velocity profile appears to be least affected. Variation at the channel centerline is in the order of 1%, increasing to approximately

3% at $y^+ = 63$. The differences between this computation and the computation with a constant $\Delta x^+ = 220$ are of similar magnitudes. The increase and decrease of the streamwise stresses when increasing/decreasing Δx agree with the results in Figs. 1 and 5. A large/small Δx gives large/small streamwise stresses. It should be noted that the evolution of the wall-normal and spanwise stresses is the reverse [6]. This is also seen in Figs. 1 and 5.

The results presented in Fig. 4 show that the stretching in the streamwise direction of a grid in a boundary layer should be kept at a minimum. This finding is a confirmation of earlier findings of Surrey [9] when doing LES of the flow around turbine blades. The results obtained above should be kept in mind when generating the grid for the airfoil.

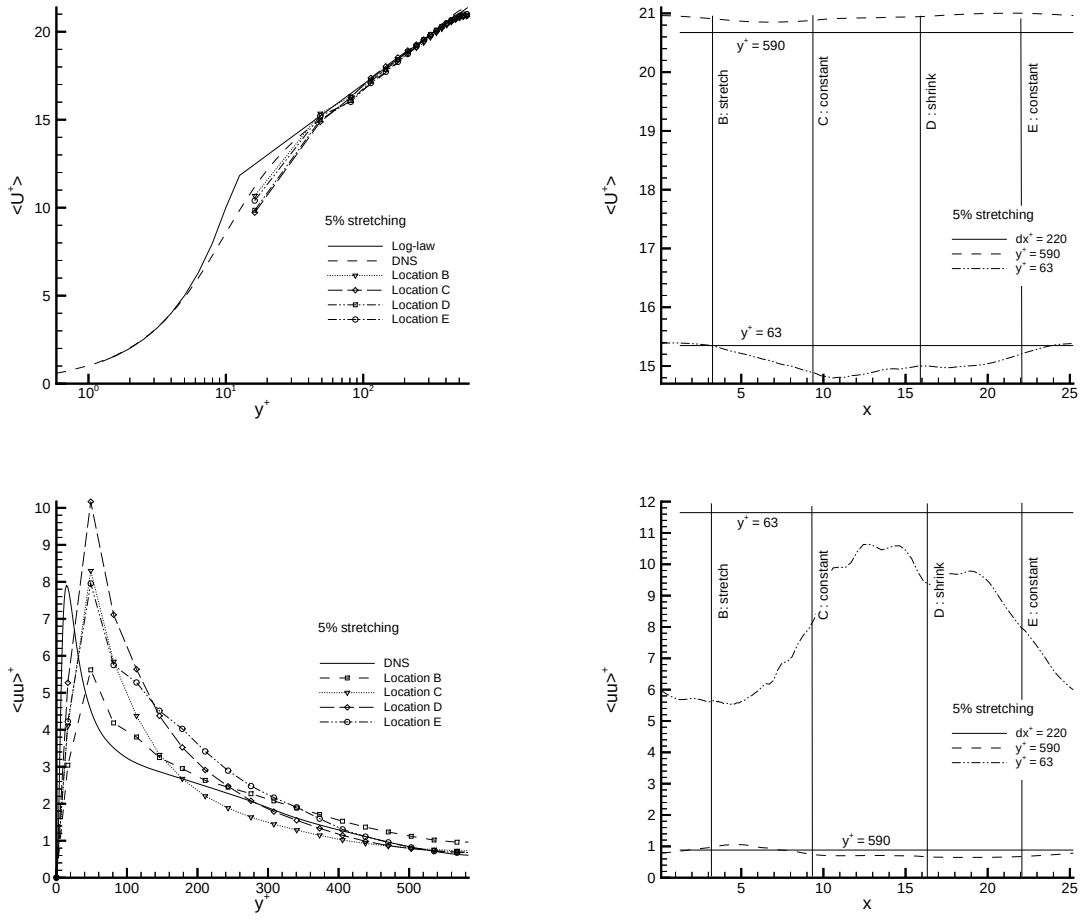

Figure 4: Channel flow, $Re_\tau = 590$. Velocity profile and streamwise normal stresses. AB and EF: $\Delta x^+ = 30$; CD: $\Delta x^+ = 220$; BC and DE: Δx^+ stretched/compressed by 5%. Solid lines in the figures to the right show predictions with constant $\Delta x^+ = 220$. Results from Ref. [6].

Some results obtained by CERFACS [10] are shown with the Werner-Wengle wall function in Fig. 5. The WALE subgrid-scale model [11] is used and several resolutions are considered. Overall, results are satisfactory, even on the coarsest grid. Of course, the peaks of velocity fluctuations cannot be properly captured, but the simulations give acceptable estimations of their amplitude. CERFACS [10] has compared, for one case ($20 \times 20 \times 20$ grid), the results obtained with a wall function based on the logarithmic law of the wall with those obtained with the Werner-Wengle wall function. Results are similar but not identical; in particular, the predicted turbulent Reynolds number shows a 6% difference between the two simulations. This is however within the range of the approximation to the logarithmic law by the power law in the Werner-Wengle wall function.

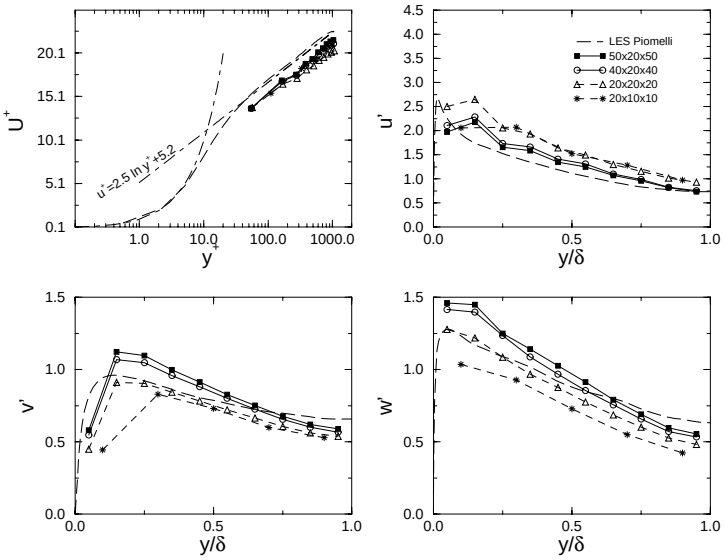

Figure 5: $Re_\tau = 1050$. Profiles of streamwise velocity and of root-mean-square velocity fluctuations in simulations with the Werner-Wengle wall function and the WALE SGS model. Resolutions are: $\Delta x^+ = 164$, $\Delta y^+ = 105$, $\Delta z^+ = 32$ ($50 \times 20 \times 50$); $\Delta x^+ = 206$, $\Delta y^+ = 105$, $\Delta z^+ = 41$ ($40 \times 20 \times 40$); $\Delta x^+ = 412$, $\Delta y^+ = 105$, $\Delta z^+ = 82$ ($20 \times 20 \times 20$); $\Delta x^+ = 412$, $\Delta y^+ = 210$; $\Delta z^+ = 164$ ($20 \times 10 \times 10$). Results from Ref. [10].

The work carried out by QMW [12] on channel flow with wall functions confirm the results obtained by CERFACS. Figure 6 compares the velocity profile obtained with the Werner-Wengle wall function with that obtained with the instantaneous logarithmic law. The predictions in Fig. 6 should be compared with the predictions of CERFACS in Fig. 5.

2.3 LES-RANS

As mentioned above, wall-resolved LES is not affordable in airfoil flow. Using wall functions is one alternative and hybrid LES-RANS is another. The method presented in

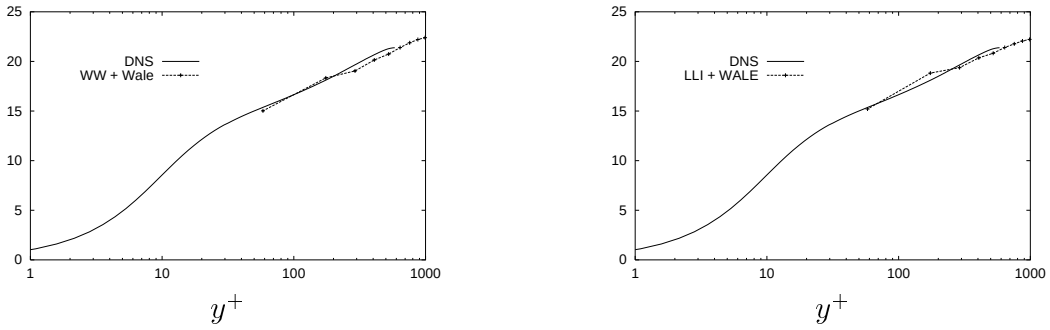

Figure 6: Velocity profiles using the Werner-Wengle wall function (left) and the instantaneous logarithmic law (right). $Re_\tau = 1050$. The WALE SGS model [11] is used. Results from Ref. [12].

[13] combines the two-equation $k-\omega$ model of Peng *et al.* [14]

$$\begin{aligned}
\frac{\partial k}{\partial t} + \frac{\partial}{\partial x_j}(U_j k) &= \frac{\partial}{\partial x_j}\left[\left(\nu + \frac{\nu_t}{\sigma_k}\right)\frac{\partial k}{\partial x_j}\right] + P_k - c_k f_k \omega k \\
\frac{\partial \omega}{\partial t} + \frac{\partial}{\partial x_j}(U_j \omega) &= \left[\left(\nu + \frac{\nu_t}{\sigma_\omega}\right)\frac{\partial \omega}{\partial x_j}\right] + \frac{\omega}{k}\left(c_{\omega 1} f_\omega P_k - c_{\omega 2} k\omega\right) + c_\omega \frac{\nu_t}{k}\left(\frac{\partial k}{\partial x_j}\frac{\partial \omega}{\partial x_j}\right) \\
\nu_t &= f_\mu \frac{k}{\omega}
\end{aligned} \tag{1}$$

with the one-equation k_{sgs} model of Davidson [3]

$$\begin{aligned}
\frac{\partial k_{sgs}}{\partial t} + \frac{\partial}{\partial x_j}(\bar{u}_j k_{sgs}) &= \frac{\partial}{\partial x_j}\left[\left(\nu + \nu_{sgs}\right)\frac{\partial k_{sgs}}{\partial x_j}\right] \\
&\quad + 2C\Delta k_{sgs}^{1/2}\bar{S}_{ij}\bar{S}_{ij} - C_*\frac{k_{sgs}^{3/2}}{\Delta} \\
\nu_{sgs} &= C_{hom}\Delta k_{sgs}^{1/2},
\end{aligned} \tag{2}$$

see also Section 2.1. The above combination has been investigated for channel flow at a Reynolds number $Re_\tau = 1050$. A mesh with $32 \times 64 \times 32$ (x, y, z) cells has been used. Different computational box sizes were used, as given in Table 1.

The matching line near the lower wall is located at y_{ml}, see Table 1. The cell below the matching line is denoted by j_{match}. At the lower matching line, the following boundary conditions are used:

$$\begin{aligned}
&j = j_{match}: \ \frac{\partial k}{\partial y} = \frac{\partial \omega}{\partial y} = 0 \\
&j = j_{match} + 1: \ \nu_{t,j_{match}+1} = \nu_{sgs,j_{match}} \ \Rightarrow k_{sgs}^{-} = \left(\frac{\nu_t}{C_{hom}\Delta}\right)^2_{j_{match}}.
\end{aligned} \tag{3}$$

k_{sgs}^{-} is the SGS kinetic energy, which is transported by convection-diffusion to the LES region. It is introduced via sources and the convection-diffusion coefficient connecting

Case	x_{max}	z_{max}	m.l. y/δ	m.l. j_{match}	m.l. y^+	Δx^+	Δz^+
1	2π	0.5π	0.023	4	25	206	52
2	2π	0.5π	0.057	8	60	206	52
3	4π	π	0.023	4	25	412	104
4	4π	π	0.057	8	60	412	104
5	4π	π	0	0	0	412	104

Table 1: Size of the computational domain and position of the matching line (m.l.) between the LES and RANS regions. The j_{match} value represents number of cells in the RANS region. Note that in Case 5 only LES is used.

the LES region to the RANS region is set to zero, i.e. $a_{S,j_{match}+1} = 0$ [13]. Results for mean velocity and shear stress are given in Fig. 7. The velocity profiles for Cases 1 and 2 (restricted computational domain) are seen to agree well with the LES benchmark. A minor kink is visible near the matching line. When the computational domain is increased (Cases 3 and 4), the agreement is not that good, although it is still much better than when only LES is used (Case 5).

The total shear stress for Case 1, Fig. 7b, varies linearly with y, as it should. The sum of SGS shear stress (RANS shear stress near the wall) and the viscous shear stress increases as the wall is approaches.

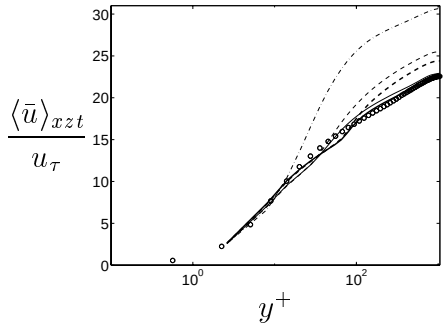

(a) Solid thin line: Case 1 (see Table 1); solid thick line: Case 2; dashed thin line: Case 3; dashed thick line: Case 4; dash-dotted line: Case 5.

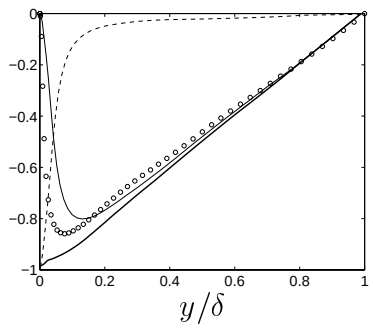

(b) Case 1. Solid thick line: total shear stress; solid thin line: resolved shear stress; dashed line: sum of SGS or RANS shear stress and viscous shear stress.

Figure 7: Channel flow. $Re_\tau = 1050$, $\Delta y^+ = 2.6 - 97$. Markers: LES by Piomelli [15]. a) $\bar{u}$ profiles. b) shear stresses. Results from Ref. [13, 16].

3 HILL FLOW

In channel flow, the flow is attached with no separation. In high-lift airfoil flow, a correct prediction of the separation region represents one of the main difficulties. With LES, we hope to be able to predict the separation region, with its large turbulent structures, more accurately than with traditional RANS methods. This is the reason why a test case with a large separation region was chosen in the LESFOIL project.

The 1995 ERCOFTAC/IAHR Workshop presented flow over a number of different hill configurations: a single hill, developing flow over a series of hills, and a periodic hill configuration. Experimental data are available for the first two cases [17]. Initial computations were performed by Karlsruhe on what was judged to be the least demanding configuration: this was the periodic hill without side walls. Based on hill height and mean centerline velocity, the Reynolds number for these calculations was $Re_h = 60\,000$, while the Reynolds number based on the height of the channel containing the hills was $Re_H = 365\,000$. It was decided to abandon this configuration, primarily because of the high computational cost of the chosen configuration and a lack of knowledge of the influence of the side walls in the experiment.

Karlsruhe led activities and tests towards defining a suitable test geometry, and a decision was taken, to define a new geometry, independent of experiments, which would provide an easily computed test case containing flow separation and reattachment. Although no experimental data would be available, the ability to perform comparative studies of wall models and SGS models was judged to be instructive and useful. To provide reference results, a wall-resolving benchmark computation using the dynamic SGS model was to be performed.

The wall-resolved LES of Karlsruhe [6, 18] are presented in Fig. 8. The grid consists of more than five million cells, and the flow was predicted employing domain decomposition on 100+ nodes on the SP machine in Karlsruhe (the numerical method is briefly described in Section 4). Furthemore, Karlsruhe [6, 18] carried out five computations employing wall functions. Three different grids and two different subgrid-scale models were used. The details of these computations are summarised in Table 2. Computations #1,2,4 & 5 assessed the impact of different SGS models and the effect of grid refinement. Computation #3 was done to assess the relationship between the spanwise correlation and the width of the domain and used a grid with $L_z = 9.0h$ instead of the usual $4.5h$. In the $x - y$ plane, this grid is identical to that used in Case #1 & 2. This computation was not progressed to a statistically converged state. All computations used the Werner-Wengle wall function to treat the near-wall region of the flow.

The grid used in Case #1 - 3 is nearly uniformly spaced. Based on the first three cases, the grid in Case #4 & 5 was refined in the streamwise direction in the area around the hill crest to better resolve the flow around the separation point. In addition, this grid is slightly stretched normal to the lower wall. All grids are uniformly spaced in the spanwise direction.

Comp #	SGS model	Grid	Integration time
1	Smag	$118 \times 66 \times 96$	~ 120 f.t.t
2	Dyn	$118 \times 66 \times 96$	~ 115 f.t.t
3	Dyn	$118 \times 66 \times 194$	~ 25 f.t.t
4	Smag	$182 \times 66 \times 96$	~ 100 f.t.t
5	Dyn	$182 \times 66 \times 96$	~ 100 f.t.t

Table 2: LES of the hill flow by Karlsruhe [6,18] using the Werner-Wengle wall functions. f.t.t. stands for flow through time.

The results obtained exhibit sensitivity to the SGS model and to the grid employed. It appears that the point of flow separation is little influenced by the choice of the subgrid model but is dependent on the amount of grid refinement around the crest of the hill. In contrast, the reattachment location is affected by both the model employed and the grid used. Refining the grid increases the separation length, while employing the dynamic SGS model instead of the Smagorinsky SGS model causes the separation length to become shorter. Generally, the fine-grid/dynamic SGS combination indicates details which are only hinted at by the other simulations.

The effects of near-wall modelling were found to be subordinate, but this is likely to be due to the fact that, over the majority of the flow domain, the points closest to the wall were located at $y^+ \leq 6$, i.e. in the viscosity-affected near-wall region. When the first point is so close to the wall, the Werner-Wengle wall function employs what is effectively a no-slip condition. Wall modelling is likely to be increasingly important as the near-wall model bridges a region greater than $y^+ = 20$.

The dynamic subgrid-scale model was found to predict levels of turbulent viscosity significantly larger than those given by the Smagorinsky model. Deviations in the other flow quantities are attributable to this difference. Near the crest of the hill at $x/h = 0.1$, the ratio $(\nu_{t,dyn}/\nu_{t,Smag})_{max}$ is approximately 3-4. Just after separation, at $x/h = 0.5$, it increases to approximately 7.5 and then, further down the channel, drops back once more to $\sim$ 3-4. Some of this can presumably be attributed to the usual uncertainty inherent in the specification of the Smagorinsky constant (here, $C_s = 0.1$ was used), though different results for different models are usual. Whether this is the only reason for the differences in ν_t is currently being investigated.

The danger of a strong spanwise correlation was one important reason for opting for the modified hill geometry. Specifically, the reduced channel height allowed a spanwise width of $4.5h$ to be used without an undue increase in the spanwise extent and resolution. In fact, the results obtained here suggest that the correlation level is in fact significant in important regions of the detached shear layer. Doubling the width of the domain, as in Case #5 produces results close to the desired correlation levels. However, a domain width of $9.0h$ leads to prohibitive computational costs.

In Fig. 8 streamlines from Case #2 are presented. It can be seen that the predicted separation region is somewhat shorter than the benchmark predictions.

Chalmers [16] has used the so-called Detached Eddy Simulation (DES) of Spalart *et al.* [19]. The grid used in the DES was fairly coarse ($56 \times 64 \times 48$). The Spalart-Allmaras one-equation RANS model is used in the near-wall boundary layer. This model reverts to a simple one-equation SGS model in regions well away from the wall by reformulating the length scale in the destruction term of this model. Following Shur *et al.*'s estimation on the model constant, C_{des}, for homogeneous turbulence, a value of $C_{des} = 0.65$ was employed in the simulation. The predicted streamlines are shown in Fig. 8. As can be seen, the recirculation region is too small. One reason may be the coarse grid, which is very coarse as compared with the wall function mesh used by Karlsruhe. It should be noted, however, that, in terms of wall units, the DES-grid is not coarse in comparison with what can be afforded in airfoil flow.

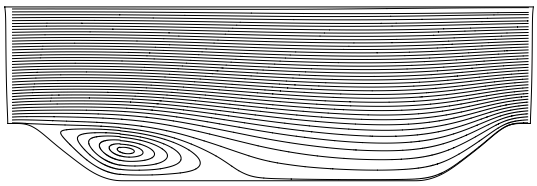

(a) Wall-resolved LES. $202 \times 130 \times 192$. Results from Ref. [6, 18].

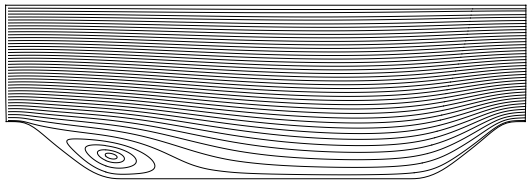

(b) LES using wall functions ($118 \times 66 \times 96$), Case #2, see Table 2. Results from Ref. [6, 18].

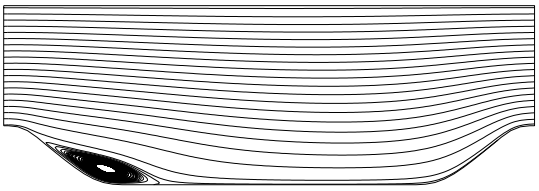

(c) DES ($56 \times 64 \times 48$). Results from Ref. [16].

Figure 8: Hill flow.

4 AIRFOIL FLOW

The A-airfoil [20–23] (see also Ref. [24]) has been chosen in the LESFOIL project. Measurements have been carried out in two different wind tunnels, F1 and F2. Skin friction and surface pressure were measured in both wind tunnels and, in the F2 wind tunnel, also detailed LDV measurements were carried out. The mean velocities and the stresses ($\overline{uv}$, $\overline{u^2}$ and $\overline{v^2}$) were measured. Detailed data exist for three angles of incidence, namely $\alpha = 7.2^o$, 12.2^o and 13.3^o at Reynolds number $2.1 \cdot 10^6$, based on the freestream

	mesh	L_z	T_{int}	SGS model	Wall function
Chalmers	$720 \times 65 \times 32$	0.08	$6c/U_\infty$	Smag. [33]	LL
CERFACS WW	$256 \times 65 \times 18$	0.036	$6.6c/U_\infty$	WALE [11]	WW
CERFACS DES	$513 \times 97 \times 18$	0.08	c/U_∞	WALE [11]	DES [19]
Karlsruhe #1	$516 \times 94 \times 70$	0.13	$5.5c/U_\infty$	Dyn [34, 35]	WW
Karlsruhe #2	$622 \times 70 \times 70$	0.13	$5.5c/U_\infty$	Dyn [34, 35]	WW
ONERA	$513 \times 97 \times 32$	0.03	$10c/U_\infty$	MILES [36, 37]	-

Table 3: Computational details for airfoil prediction. Different spanwise extent L_z, integration time T_{int} and SGS models. Two different wall functions were used, the Werner-Wengle (WW) [7] and the instantaneous log law (LL).

velocity and the chord length. In the LESFOIL project we focus on high-lift airfoils and have thus chosen the highest angle of incidence, $\alpha = 13.3^o$. For this flow, a small separation bubble close to the trailing edge prevails, according to experiments.

Computations from the following partners are presented below: Chalmers [25, 26], CERFACS [27], Karlsruhe [28] and ONERA [29]. Some computational details are given in Table 3. Below, some earlier work by CERFACS is also included [30, 31] (see also Ref. [32]). As can be seen in Table 3, CERFACS used the DES method. However, the time integration was very short, and thus the results are preliminary. All meshes except in ONERA's and the CERFACS' DES computations were "wall function meshes", i.e. the near-wall nodes are located in the neighborhood of $y^+ = 30$.

All four partners use finite volume technique. Chalmers employs an implicit finite volume method with central differencing in space and Crank-Nicolson in time. The code employs a pressure correction scheme (PISO). The code is parallelized using domain decomposition [38]. On 32 processors of the IBM SP in Stockholm, the computations, on the mesh described in Table 3, are advanced by $4.3c/U_\infty$ over 24 hours (elapsed time).

The airfoil calculations undertaken by CERFACS were performed using the parallelized multi-block flow solver NSMB. The numerical scheme is fourth order accurate in each direction [39] (overall, formally only second order) together with the "wiggle detector" and implicit time integration. A dual-time stepping method is used with a Crank-Nicholson scheme for the outer loop and Newton subiterations to ensure time accuracy. Using the wall function mesh in Table 3 ($256 \times 65 \times 18$), 72 hours (elapsed time) on eight processors of an SGI ORIGIN 2000 are required to advance the solution by c/U_∞.

Karlsruhe employs the LESOCC finite volume code, parallelised by domain decomposition and explicit message passing [40]. This code uses a collocated discretisation and curvilinear coordinates with second order central schemes in space and Runge-Kutta time stepping. The SIMPLE procedure is used for the pressure-velocity coupling. Using 48 processors of the IBM RS/6000 SP in Karlsruhe the solution is advanced by approximately by $2.4c/U_\infty$ over 24 hours of elapsed time.

ONERA employs an implicit finite volume method. A second order accurate BDF

scheme is used for the temporal discretization, whereas the non-linear problem is solved by an approximate Newton method. The convective fluxes are approximated by a second-order upwind-biased scheme. The required CPU time for c/U_∞ is 6 hours on a NEC SX5 (one processor).

To investigate the relation of the numerical dissipation associated with upwind schemes and the SGS dissipation, computations have been carried out by ONERA without the use of explicit SGS models. The SGS dissipation is assumed to be provided by the numerical dissipation. This approach is often referred to as the MILES approach [36, 37], which is known to give reliable results for complex geometries. ONERA has undertaken some computations for several values of the angle of attack in order to assess the reliability of the MILES approach for non-separated cases. Preliminary results seem to indicate that the MILES approach is able to (i) recover the transition process and (ii) yield realistic values of the aerodynamics parameters of the profile.

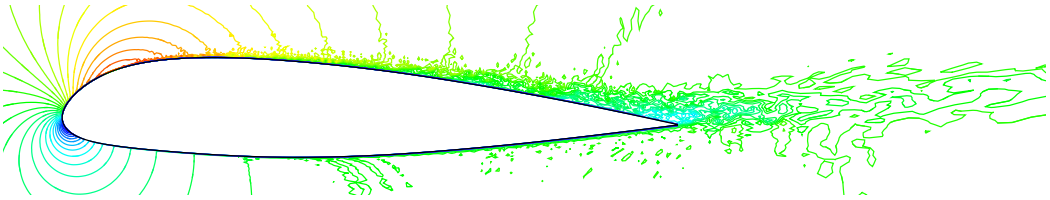

Figure 9: Instantaneous $\bar{u}$ velocity. Results from Ref. [25, 26].

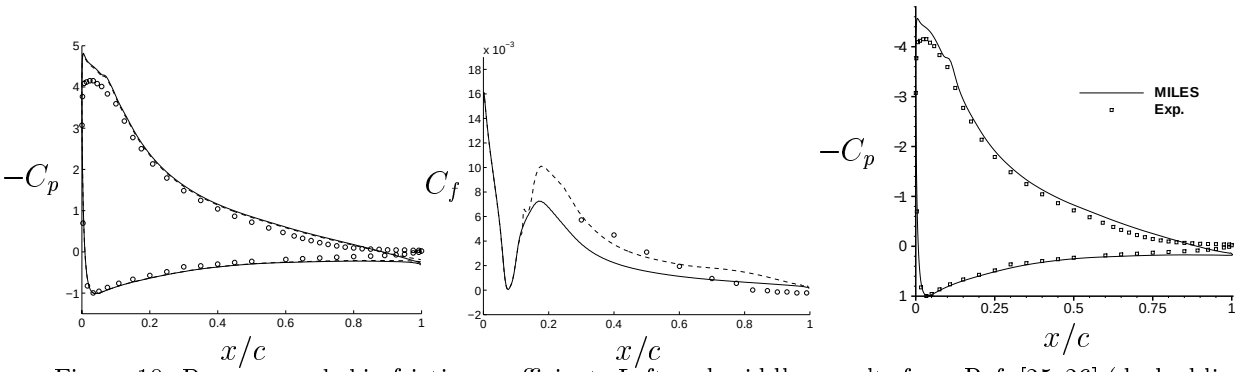

Figure 10: Pressure and skin friction coefficient. Left and middle: results from Ref. [25, 26] (dashed lines: wall functions; solid lines: no-slip conditions); right: results from Ref. [29].

4.1 Transition

The flow along the airfoil undergoes transition from laminar to turbulent flow on the suction side and on the pressure side. The transition on the suction side is, from a numerical point of view, by far the most crucial. In the experiments, the flow is tripped at

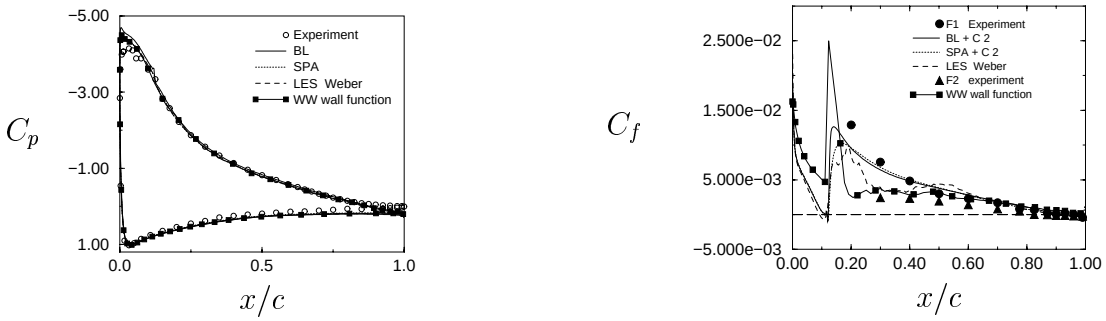

Figure 11: Pressure and friction coefficients. BL+C2: 2D RANS emplying Balwdin-Lomax and second-order central differencing; SPA+C2: 2D RANS Spalart-Allmaras model and second-order central differencing (identical to DES). Results from Ref. [27, 30, 31].

the pressure side at $x/c = 0.3$ and the transition takes place at the suction side – without triggering – at $x/c \simeq 0.12$. Although dynamic SGS models have successfully been used to predict transition at low Reynolds numbers [41], it is not feasible to *predict* transition at the A-airfoil due to the high Reynolds number. In the LESFOIL project, attention has been given on how to *prescribe* transition at the locations found (or tripped) in the experiments. Chalmers, CERFACS and Karlsruhe all had the same experience: using central differencing in the region upstream of the airfoil resulted in unphysical oscillations due to insufficient SGS dissipation. The remedy used by Chalmers and Karlsruhe was to employ a bounded second-order discretization scheme for the convective terms upstream of the transition. At the locations of transition, the upwind scheme is switched (a blend is used by Chalmers) to central differencing, after which (numerical) transition automatically takes place.

CERFACS takes care of the unphysical oscillations upstream of the airfoil by employing an artificial viscosity [39] (a fourth-order operator) to smooth the flow in regions where spurious oscillations such as wiggles are detected. This "wiggle detector" is thus able to reduce the artificial damping in situations in which no oscillation develops.

An example of the instantaneous flow is shown in Fig. 9. As can be seen, almost no oscillations are present in the region upstream of the locations of transition ($x/c = 0.12$ on the suction side and $x/c = 0.3$ on the pressure side). Careful inspection of the flow along the suction side reveals also some numerical oscillations upstream of the location of transition, although mostly in the region in which the blending between upwind and central differencing is applied. Oscillations are present downstream of the locations of transition. Hopefully, most of these are physical, but there are bound also to be unphysical, numerical oscillations. The boundary layer on the suction side is intentionally much better resolved than the one on the pressure side.

Problems are still experienced by Chalmers and Karlsruhe concerning the numerical tripping of the boundary layer at the suction side. It seems that, by switching from the bounded second-order upwind scheme to the central differencing scheme, the turbulence experiences a "hard kick" and, as a result, the transition takes place in an explosive,

unphysical manner.

It should be mentioned that in Surrey's computations [42], the problems concerning transition are reversed: the flow does not become turbulent, and no transition takes place automatically. No oscillations appear, although pure central differencing is used everywhere. The reason is probably that the code used by Surrey is more dissipative than those used by Chalmers, CERFACS and Karlsruhe. Surrey is attempting to trip transition by imposing disturbances in the wall-normal momentum equation.

4.2 Turbulent Flow

The results have been averaged in time (T_{int} is given in Table 3) and in the spanwise direction, denoted by $\langle . \rangle_{zt}$.

Figures 10, 11 and 14 present pressure and skin friction coefficients. It can be seen from the C_p-curves that the pressure does not level off at the suction side when the trailing edge is approached, indicating that no separation is taking place. The story is the same in the skin friction coefficients: they do not become negative. It could be tempting to interpret the suction peak seen at the suction side as a problem rooted in inaccurate prediction of the flow in the leading edge region. Although there certainly *are* problems in the transition region, the experience gained in earlier European projects on RANS simulations of the A-airfoil [24, 43] (see also Refs. [44, 45]) has shown that failure in predicting separation in the trailing edge region is related to excessively high suction peaks. Still, it should be remembered that the fact that separation is not captured, may be due to an inaccurate prediction of the developing boundary layer approaching the trailing edge. If this is the case, then the inaccurate prediction may have its origin in an inappropriate treatment of the transition. Thus, the over-prediction of the suction peak can indirectly be the consequence of inaccurate prediction of the flow in the leading edge region.

Figures 12, 13 and 14 present predicted velocity and shear stress profiles. Please note that the velocities and stresses have been transformed to a local $s-n$ coordinate system, where s is tangential to the local suction surface and n is the wall-normal direction. As can be seen, the velocity is already too high at $x/c = 0.3$ (Fig. 12), which is connected to the excessively high suction peak. Further downstream, the velocity profiles are too full (Figs. 12, 13 and 14) and no tendency toward separation is seen. The fact that the velocity profiles are too full is usually related to excessively large shear stresses, producing too high turbulent, diffusive wall-normal transport of streamwise momentum. As can be seen in Fig. 12, the shear stresses are not too large as compared with the experimental values but rather the opposite. However, care should always be exercised when comparing computed and experimental stresses, when the computed and the experimental velocity field do not agree. As can be seen in Fig. 12, the experimental velocity gradients are larger than the predicted ones. Thus, large experimental shear stresses are generated, which explains why the experimental shear stresses are larger than the predicted ones, although the predicted velocity profiles are fuller than the experimental velocity profiles.

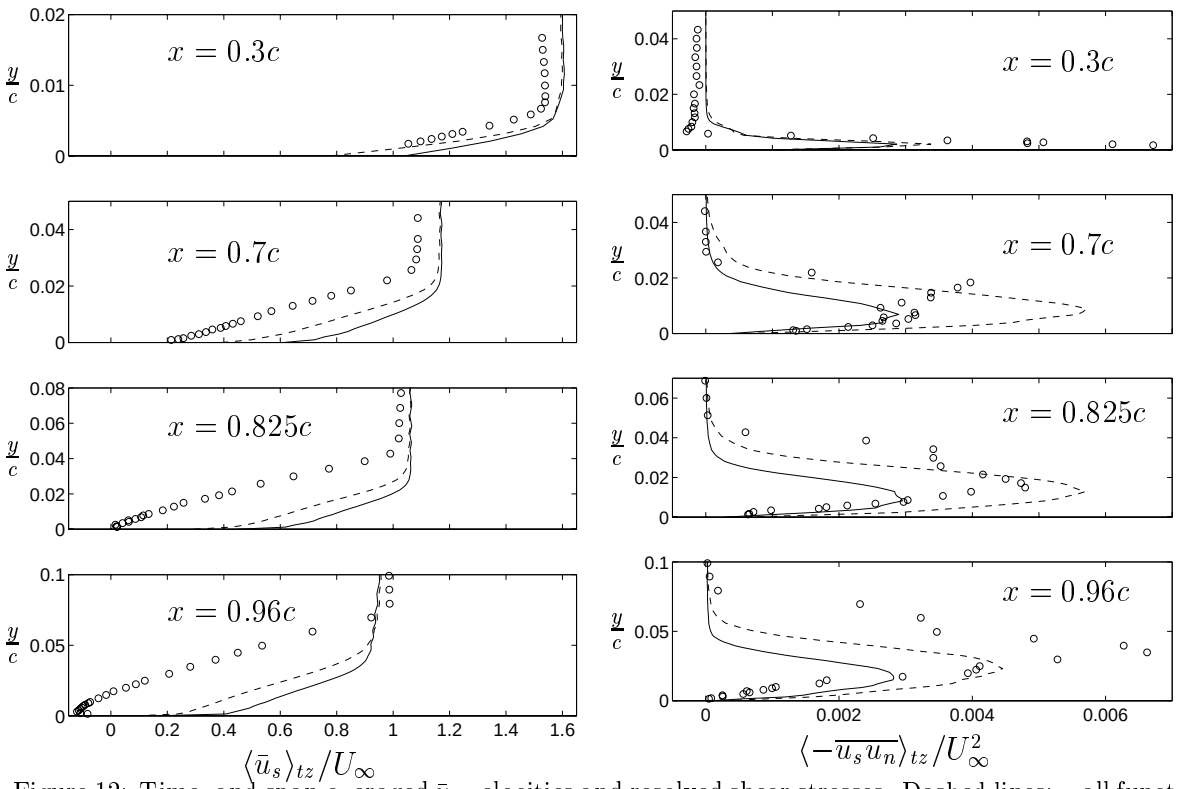

Figure 12: Time- and span-averaged $\bar{u}_s$ velocities and resolved shear stresses. Dashed lines: wall functions (see Table 3); solid lines: no-slip conditions. Results from Ref. [25, 26].

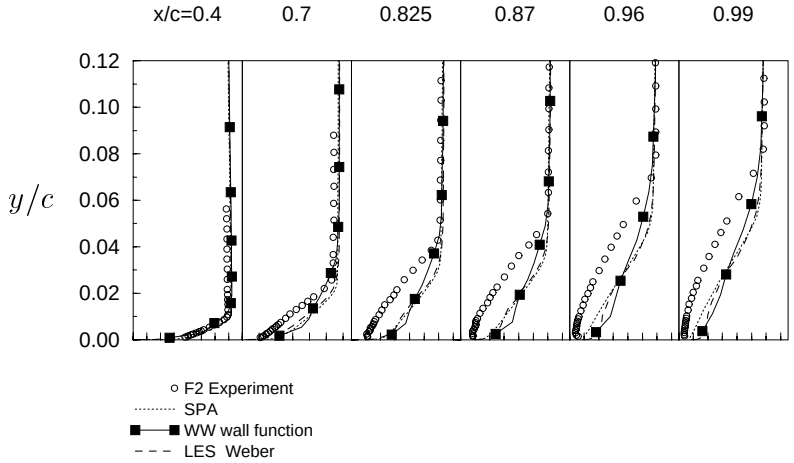

Figure 13: Time- and span-averaged $\bar{u}_s$ velocities. Dotted lines (SPA): DES from Ref. [27]; dashed line (LES Weber): results from Ref. [30, 31]; solid line with black markers (WW wall function): results from Ref. [27].

5 CONCLUSIONS

In the LESFOIL project, parallelized, numerical methods have been refined and developed and SGS models and near-wall models have been developed and evaluated in

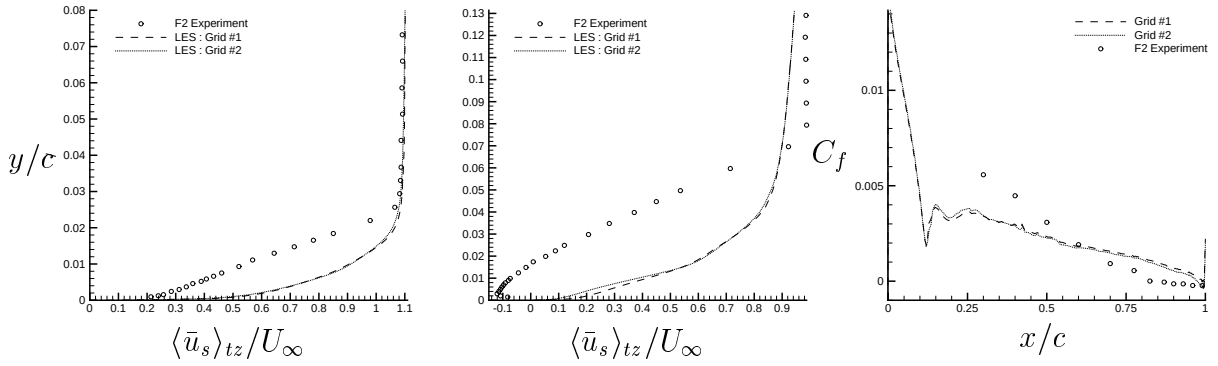

Figure 14: Velocity profiles and skin friction. Left: $x/c = 0.7$; middle: $x/c = 0.96$. Results from Ref. [28].

channel flow and recirculating flow in a channel with a hill. Much has been learnt on the behaviour of wall models in simple flows and the required grid resolution. The LES carried out for the flow around the Aerospatiale A-airfoil are, however, so far rather disappointing. The separation region, which according to experiments should prevail in the trailing edge region, is not predicted.

There are still some problems on how to *impose* transition in a correct way to allow an accurate prediction of the developing boundary layer on the suction side. Further work will also be carried out on wall functions and on hybrid LES-RANS and DES.

Acknowledgment

The LESFOIL project (Project No. BRPR-CT97-0565) is financed by the Brite-Euram programme.

References

[1] P. Moinat and F. Ducros. CERFACS' 12-month report, LESFOIL: A Brite-Euram project. Technical report, CERFACS, Toulouse, France, 1999.

[2] U. Piomelli and J. Liu. Large-eddy simulation of rotating channel flow using a localized dynamic model. *Physics of Fluids A*, 7:839–848, 1995.

[3] L. Davidson. Large eddy simulation: A dynamic one-equation subgrid model for three-dimensional recirculating flow. In *11th Int. Symp. on Turbulent Shear Flow*, volume 3, pages 26.1–26.6, Grenoble, 1997.

[4] A. Sohankar, L. Davidson, and C. Norberg. Large eddy simulation of flow past a square cylinder: Comparison of different subgrid scale models. *ASME: Journal of Fluids Engineering*, 122(1):39–47, 2000.

[5] S. Dahlström and L. Davidson. Chalmers' 12-month report, LESFOIL: A Brite-Euram project. Technical report, Dept. of Thermo and Fluid Dynamics, Chalmers University of Technology, Gothenburg, 1999.

[6] C. Mellen, J. Fröhlich, and W. Rodi. Karlruhe's 18-month report, LESFOIL: A Brite-Euram project. Technical report, Institut für Hydrodynamik, University of Karlsruhe, Germany, 1999.

[7] H. Werner and H. Wengle. Large-eddy simulation of turbulent flow over and around a cube in a plane channel. In *Turbulent Shear Flows 8*, pages 155–168. Springer-Verlag, 1991.

[8] R.D. Moser, J.D. Kim, and N.N. Mansour. Direct numerical simulation of turbulent channel flow up to $Re_\tau = 590$. *Physics of Fluids A*, 11:943–945, 1999.

[9] T. Gough, S. Gao, P. Hancock, and P.R. Voke. Experiment and simulation of the tripped boundary layer on a flat plate: Comparative study. Technical Report ME-FD/95.40, Department of Mechanical Engineering, The University of Surrey, U.K., 1996.

[10] F. Ducros and P. Moinat. CERFACS' 18-month report, LESFOIL: A Brite-Euram project. Technical report, CERFACS, Toulouse, France, 1999.

[11] F. Ducros, F. Nicoud, and T. Poinsot. Wall-adapting local eddy-viscosity models for simulations in complex geometries. In *6th ICFD Conference on Numerical Methods for Fluid Dynamic*, pages 293–299, 1998.

[12] M.A. Leschziner and L. Temmerman. QMW's 24-month report, LESFOIL: A Brite-Euram project. Technical report, Department of Engineering, Queen Mary & Westfield College, University of London, 2000.

[13] L. Davidson. LES-RANS of channel flow. Technical Report 00/2, Dept. of Thermo and Fluid Dynamics, Chalmers University of Technology, Gothenburg, Sweden, 2000.

[14] S-H Peng, L. Davidson, and S. Holmberg. A modified Low-Reynolds-Number $k-\omega$ model for recirculating flows. *ASME: Journal of Fluids Engineering*, 119:867–875, 1997.

[15] U. Piomelli. High Reynolds number calculations using the dynamic subgrid-scale stress model. *Physics of Fluids A*, 5:1484–1490, 1993.

[16] S.-H Peng and L. Davidson. Chalmers' 24-month report, task 2, LESFOIL : A Brite-Euram project. Technical report, Dept. of Thermo and Fluid Dynamics, Chalmers University of Technology, Gothenburg, 2000.

[17] M.V. Almeida, D.F.G. Durau, and M.V. Heitor. Wake flows behind two-dimensional hills. *Exp. Thermal and Fluid Science*, 7:87, 1993.

[18] C.P. Mellen, J. Frölich, and W. Rodi. Large eddy simulation of the flow over periodic hills. In *16th IMACS World Congress 2000, Lasaunne, August 21-25*, 2000.

[19] M. Shur, P.R. Spalart, M. Strelets, and A. Travin. Detached-eddy simulation on an airfoil at high angle of attack. In W. Rodi and D. Laurence, editors, *Engineering Turbulence Modelling and Experiments 4*, pages 669–678. Elsevier, 1999.

[20] A.M. Rodde. Opération décrochage – exploitation des essais à F1 sur les profils A et B. Technical Report RSF No 74/1685 AYG, ONERA, 1987.

[21] R. Huddeville, O. Piccin, and D. Cassoudesalle. Opération décrochage – mesurement de frottement sur profils AS239 et A240 à la soufflerie F1 du CFM. Technical Report RT-OA 19/5025 (RT-DERAT 19/5025 DN), ONERA, 1987.

[22] Ch. Gleyzes. Opération décrochage – résultats des essais à la soufflerie F2. Technical Report RT-DERAT 55/4004, ONERA, 1988.

[23] Ch. Gleyzes. Opération décrochage – résultats de la 2ème campagne d'essai à F2 – mesures de pression et vélocimétrie laser. Technical Report RT-DERAT 55/5004, ONERA, 1989.

[24] E. Chaput. Application oriented synthesis – Aerospatiale A-airfoil. contribution in ECARP: European computational aerodynamics research project : Validation of CFD codes and assessment of turbulence models. In W. Haase *et al.*, editor, *Notes on Numerical Fluid Mechanics*, volume 58, pages 327–346. Vieweg Verlag, 1996.

[25] S. Dahlström and L. Davidson. Chalmers' 24-month report, task 5, LESFOIL : A Brite-Euram project. Technical report, Dept. of Thermo and Fluid Dynamics, Chalmers University of Technology, Gothenburg, 2000.

[26] S. Dahlström and L. Davidson. Large eddy simulation of the flow around an Aerospatiale A-aerofoil. In *ECCOMAS 2000, European Congress on Computational Methods in Applied Sciences and Engineering, 11-14 September*, Barcelona, Spain, 2000.

[27] F. Ducros. CERFACS' 24-month report, LESFOIL: A Brite-Euram project. Technical report, CERFACS, Toulouse, 2000.

[28] C. Mellen, J. Fröhlich, and W. Rodi. Karlruhe's 24-month report, LESFOIL: A Brite-Euram project. Technical report, Institut für Hydrodynamik, University of Karlsruhe, Germany, 2000.

[29] P. Sagaut and I. Mary. ONERA's 24-month report, LESFOIL: A Brite-Euram project. Technical report, ONERA, Paris, 2000.

[30] C. Weber. Développement de méthodes implicites pour les équations de Navier-Stokes moyennées et la simulation des grandes échelles: application à l'aérodynamique externe. thèse, INPT, Toulouse, France, 1998.

[31] C. Weber, F. Ducros, and A. Corjon. Large-eddy simulation of complex turbulent flows. AIAA paper 92-0439, Reno, NV, 1991.

[32] C. Weber and F. Ducros. Large eddy and Reynolds-averaged Navier-Stokes simulations of turbulent flow over an airfoil. *International Journal of Computational Fluid Dynamics (submitted)*, 2000.

[33] J. Smagorinsky. General circulation experiments with the primitive equations. *Monthly Weather Review*, 91:99–165, 1963.

[34] M. Germano. Turbulence: the filtering approach. *Journal of Fluid Mechanics*, 238:325–336, 1992.

[35] D.K. Lilly. A proposed modification of the Germano subgrid-scale closure method. *Physics of Fluids A*, 4:633–635, 1992.

[36] J.P. Boris, F.F. Grinstein, E.S. Oran, and R.L. Kolbe. New insights into large eddy simulation. *Fluid Dynamic Research*, 10:199–228, 1992.

[37] E. Garnier, M. Mossi, P. Sagaut, P. Comte, and M. Deville. On the use of some shock capturing schemes for large-eddy simulation. *Journal Computational Physics*, 153:273–311, 1999.

[38] H. Nilsson and L. Davidson. CALC-PVM: A parallel multiblock SIMPLE multiblock solver for turbulent flow in complex domains. Technical Report 98/12, Dept. of Thermo and Fluid Dynamics, Chalmers University of Technology, Gothenburg, 1998.

[39] F. Ducros, C. Soulères, F. Laporte, P. Moinat, C. Weber, and V. Guinot. High-order skew-symmetric Jameson schemes for unsteady compressible flow. In P.V. Voke, N.D. Sandham, and L. Kleiser, editors, *Direct and Large-Eddy Simulation III*, pages 417–428. Kluwer, 1999.

[40] F. Mathey, J. Fröhlich, and W. Rodi. Large eddy simulation of the flow over a matrix of surface mounted cubes. In *Lecture Notes in Physics*, volume 529, pages 153–163. Springer, 1999.

[41] F. Ducros, P. Comte, and M. Lesieur. Large-eddy simulation of transition to turbulence in a boundary layer developing spatially over a flat plate. *Journal of Fluid Mechanics*, 326:1–36, 1995.

[42] L. Jervase and P. Voke. Surrey's 24-month report, LESFOIL: A Brite-Euram project. Technical report, Department of Mechanical Engineering, The University of Surrey, U.K., 2000.

[43] EUROVAL: A European initiative on validation of CFD-codes. In W. Haase *et al.*, editor, *Notes on Numerical Fluid Mechanics*, volume 42. Vieweg Verlag, 1993.

[44] L. Davidson. Prediction of the flow around an airfoil using a Reynolds stress transport model. *ASME: Journal of Fluids Engineering*, 117:50–57, 1995.

[45] F.S. Lien and M.A. Leschziner. Modelling of 2D separation from high-lift aerofoils with a non-linear eddy-viscosity model and second-moment closure. *The Aeronautical Journal*, 99:125–144, 1995.